Ab Initio Calculations of the Stoichiometric Rutile (110) Surface

BACHELORARBEIT

zur Erlangung des akademischen Grades
Bachelor of Science (B. Sc.)
im Fach Physik

eingereicht an der
Mathematisch-Naturwissenschaftlichen Fakultät
Institut für Physik
Humboldt-Universität zu Berlin

von
Herr Marcus Fenner
geboren am 05.01.1990 in Berlin

Gutachter:

1. *Prof. Dr. Dr. h.c. Claudia Draxl*
2. *Priv.-Doz. Dr. Pasquale Pavone*

Betreuung:

1. *Nora Illanes, M.Sc.*

eingereicht am: *15. August 2014*

Contents

List of Figures

List of Tables

Chapter 1

Motivation

Titanium dioxide (TiO_2) in the rutile form is one of the most extensively researched oxide crystal. Its (110) surface has also been subject to various density functional theory (DFT) calculations for more than ten years. This makes it a perfect test bed to compare the program **exciting** with other DFT codes and experimental results.

TiO_2 – also known as titania – has a wide range of applications. For a long time it has been used as white pigment because of its high refractivity. Because it is non-toxic it has been used as a food paint[1] and in pharmaceuticals[2]. It has photocatalytic properties which have been used for splitting water[3, 4], oxidizing organic matter[5, 6], water purification[7] and sterilisation[8]. In the emerging field of hybrid organic-inorganic semiconductors TiO_2 has become a very promising candidate. It has been used for hybrid solar cells with Poly(3-hexylthiophen-2,5-diyl) (P3HT)[9–11].

To model the catalytic properties and hybrid interfaces a good understanding of the surface and its structure is needed.

Obtaining a relaxed surface structure and surface energies is the goal of this thesis.

Chapter 2

Introduction

2.1 Density Functional Theory

A non-relativistic, stationary many-electron quantum system is described by Schrödinger's equation

$$\hat{H}\Psi\left(\mathbf{r}_1, \mathbf{r}_2, \ldots, \mathbf{r}_N\right) = E\Psi\left(\mathbf{r}_1, \mathbf{r}_2, \ldots, \mathbf{r}_N\right) \tag{2.1}$$

with the position vectors $\{\mathbf{r}_i\}$ of the N electrons and the Hamiltonian

$$\hat{H} = \hat{T} + \hat{V} + \hat{U}. \tag{2.2}$$

The terms of the Hamiltonian are the kinetic energy

$$\hat{T} = -\sum_{i=1}^{N} \nabla_i^2 \tag{2.3}$$

with the Laplacian ∇^2, the external potential usually given by the electron-nucleus Coulomb attraction

$$\hat{V} = \sum_{i=1}^{N} v\left(\mathbf{r}_i\right), \tag{2.4}$$

and the electron-electron interaction

$$\hat{U} = \frac{1}{2}\sum_{i=1}^{N}\sum_{j\neq i}^{N} \frac{e^2}{|\mathbf{r}_i - \mathbf{r}_j|}. \tag{2.5}$$

As a result the wave function depends on $3N$ coordinates and it is therefore not feasible to calculate many-electron systems.

However Hohenberg and Kohn[12] showed that the ground-state wave function is a unique functional of the ground-state density n_0

$$\Psi_0 = \Psi\left[n_0\right] \tag{2.6}$$

with

$$\begin{aligned} n_0\left(\mathbf{r}\right) &= \left\langle \Psi_0 \left| \sum_{i=1}^{N} \delta\left(\mathbf{r} - \mathbf{r}_i\right) \right| \Psi_0 \right\rangle \\ &= N \int \mathrm{d}^3 r_2 \int \mathrm{d}^3 r_3 \cdots \int \mathrm{d}^3 r_N \Psi_0^*\left(\mathbf{r}, \mathbf{r}_2, \ldots, \mathbf{r}_N\right) \Psi_0\left(\mathbf{r}, \mathbf{r}_2, \ldots, \mathbf{r}_N\right). \end{aligned} \tag{2.7}$$

This is known as the first Hohenberg-Kohn theorem. The expectation value of an observable $\hat{O}$ is thus a functional of the ground-state density

$$\left\langle \Psi[n_0] \left| \hat{O} \right| \Psi[n_0] \right\rangle = O\left[n_0\right]. \tag{2.8}$$

For example the expectation value of an external potential can be written as

$$\left\langle \Psi \left| \hat{V} \right| \Psi \right\rangle = V\left[n\right] = \int \mathrm{d}^3 r \, v\left(\mathbf{r}\right) n\left(\mathbf{r}\right). \tag{2.9}$$

The energy of the system can therefore be expressed as

$$E\left[n\right] = T\left[n\right] + U\left[n\right] + \int \mathrm{d}^3 r \, v\left(\mathbf{r}\right) n\left(\mathbf{r}\right). \tag{2.10}$$

The second theorem states that the energy takes its minimum at the ground state density.

$$E_0 = \min_{\Psi \to n_0} \left\langle \Psi \left| \hat{T} + \hat{U} + \hat{V} \right| \Psi \right\rangle. \tag{2.11}$$

Instead of having to solve a wave function for $3N$ coordinates one only has to determine the ground-state density. However it still depends on the many-electron kinetic energy and electron-electron interaction operator.

The electron-electron interaction and kinetic energy from Equation 2.10 can also be written as

$$T\left[n\right] + U\left[n\right] = T_s\left[n\right] + V_{\mathrm{H}}\left[n\right] + E_{\mathrm{XC}}\left[n\right] \tag{2.12}$$

where T_s is the independent particle kinetic energy and V_{H} the classical Coulomb or Hartree energy

$$V_{\mathrm{H}}\left[n\right] = \frac{1}{2} \iint \frac{n\left(\mathbf{r}\right) n\left(\mathbf{r}'\right)}{\left|\mathbf{r} - \mathbf{r}'\right|} \, \mathrm{d}^3 r \mathrm{d}^3 r'. \tag{2.13}$$

The difference between $T\left[n\right] + U\left[n\right]$ and $T_s\left[n\right] + V_{\mathrm{H}}\left[n\right]$ is now stored in the exchange-correlation functional $E_{\mathrm{XC}}\left[n\right]$.

By varying this equation with respect to the density, Kohn and Sham[13] derived an auxiliary system which yields the same density

$$\left[-\frac{\hbar^2}{2m} \nabla^2 + \hat{V}_{\mathrm{eff}}\left(\mathbf{r}\right) \right] \varphi_i\left(\mathbf{r}\right) = \varepsilon_i \varphi_i\left(\mathbf{r}\right) \tag{2.14}$$

with $\hat{V}_{\mathrm{eff}}$ determined by v_{eff} as in Equation 2.9. From Equation 2.14 one obtains a set of orbitals $\{\varphi_i\}$ from which one can produce the density of the original system

$$n_{\mathrm{eff}}\left(\mathbf{r}\right) = \sum_{i=1}^{N} \left|\varphi_i\left(\mathbf{r}\right)\right|^2 \equiv n\left(\mathbf{r}\right). \tag{2.15}$$

The effective potential is given by

$$v_{\mathrm{eff}}\left(\mathbf{r}\right) = v_{\mathrm{ext}}\left(\mathbf{r}\right) + e^2 \int \frac{n\left(\mathbf{r}\right)}{\left|\mathbf{r} - \mathbf{r}'\right|} \, \mathrm{d}^3 r' + \frac{\delta E_{\mathrm{XC}}\left[n\right]}{\delta n\left(\mathbf{r}\right)} \tag{2.16}$$

The total energy of the auxiliary system is

$$\begin{aligned} \Sigma\left[n\right] &= \sum_{i=1}^{N} \varepsilon_i \\ &= T_s\left[n\right] + V_{\mathrm{eff}}\left[n\right] \\ &= T_s\left[n\right] + V_{\mathrm{ext}}\left[n\right] + 2V_{\mathrm{H}}\left[n\right] + \int \frac{\delta E_{\mathrm{XC}}\left[n\right]}{\delta n\left(\mathbf{r}\right)} \, \mathrm{d}^3 r \end{aligned} \tag{2.17}$$

Comparing Equations 2.10, 2.12, and 2.17 we see that the total energy of the real system can be expressed as

$$\begin{aligned} E[n] &= T_s[n] + \frac{1}{2}\iint \frac{n(\mathbf{r})\, n(\mathbf{r}')}{|\mathbf{r}-\mathbf{r}'|}\, \mathrm{d}^3r \mathrm{d}^3r' + E_{\mathrm{XC}}[n] \\ &= \Sigma[n] - V_{\mathrm{H}}[n] + E_{\mathrm{XC}}[n] - \int \frac{\delta E_{\mathrm{XC}}[n]}{\delta n(\mathbf{r})}\, \mathrm{d}^3r \\ &= \sum_{i=1}^{N} \varepsilon_i - V_{\mathrm{H}}[n] + E_{\mathrm{XC}}[n] - \int \frac{\delta E_{\mathrm{XC}}[n]}{\delta n(\mathbf{r})}\, \mathrm{d}^3r \end{aligned} \tag{2.18}$$

If n is the ground-state density n_0 obtained by self-consistent solution of equation 2.14, Equation 2.18 gives the ground-state energy.

2.1.1 Exchange-Correlation Functionals

Equation 2.18 is exact and therefore yields the energy of the real system. However the correlation potential is only known for the homogeneous electron gas and the exchange (Hartree-Fock) potential is very difficult to compute. Therefore approximations have to be used.

The most natural choice of an exchange-correlation functional is to assume an homogeneous electron gas for which exchange is easy to compute and correlation is known in the low and high density limit and can therefore be interpolated. This approximation is the local density approximation (LDA).

$$E_{\mathrm{XC}}^{\mathrm{LDA}}[n] = \int \varepsilon_{\mathrm{XC}}^{\mathrm{hom}}(n(\mathbf{r}))\, n(\mathbf{r})\, \mathrm{d}^3r \tag{2.19}$$

$\varepsilon_{\mathrm{XC}}^{\mathrm{hom}}$ is not a functional of the density but only depends on the value of n at point $\mathbf{r}$.

General Gradient Approximation

The generalized gradient approximations (GGA) is an improvement on the LDA by using not only the local density but also the gradient of the density.

$$E_{\mathrm{XC}}^{\mathrm{GGA}}[n] = \int f(n, \nabla n)\ \mathrm{d}^3r \tag{2.20}$$

Those GGAs can be either constructed empirically by fitting parameters to known problems or non-empirically by fulfilling certain properties like scaling laws and sum rules.

2.2 exciting

exciting[1] is a full-potential all-electron DFT package. It uses the linearized augmented planewave (LAPW) method. Contrary to many other DFT codes it does not use pseudo-potentials but instead considers all electrons explicitly.

exciting uses atomic units which will be used in the following figures:

$$1\, E_{\mathrm{h}} = 1\ \mathrm{Ha} = 27.211\,383\,86(68)\ \mathrm{eV}$$

[1] `http://exciting-code.org/`

$$1\,a_0 = 0.529\,177\,208\,59(36)\ \text{Å}$$
$$\hbar, m_e, e = 1$$

2.2.1 Structure Relaxation

The structure optimisation or relaxation is the optimisation of the atomic positions without changing the lattice parameters. This is done by calculating the forces that act on the atoms and shifting their position until they are below a certain threshold.

For structure relaxation **exciting** can use three different methods:

- `newton`
- `harmonic`
- `BFGS`

Newton Method

In the Newton method an atom α is displaced according to

$$\mathbf{r}_\alpha^{(m+1)} = \mathbf{r}_\alpha^{(m)} + \tau_\alpha^{(m+1)} \left(\mathbf{F}_\alpha^{(m)} + \mathbf{F}_\alpha^{(m-1)}\right) \tag{2.21}$$

in each optimisation step m. The magnitude of the displacement is determined by the forces $\mathbf{F}$ acting on the atoms and the parameter τ_α.

Harmonic Method

The harmonic method uses the Newton method unless the 'harmonic condition'

$$\beta = \frac{F_\alpha^{(m-1)}}{F_\alpha^{(m)}} \notin]0, 3[\tag{2.22}$$

is fulfilled. In this case the atoms are displaced according to

$$\mathbf{r}_\alpha^{(m+1)} = \frac{\mathbf{r}_\alpha^{(m-1)} - \beta \mathbf{r}_\alpha^{(m)}}{1 - \beta} \tag{2.23}$$

BFGS

The Broyden–Fletcher–Goldfarb–Shanno (BFGS) algorithm for solving nonlinear optimisation problems is a quasi-Newton method proposed independently by Broyden[14], Fletcher[15], Goldfarb[16], and Shanno[17].

For quasi-Newton methods one uses the Taylor series

$$F\left(\mathbf{r}_m + \Delta\mathbf{r}\right) \approx F\left(\mathbf{r}_m\right) + \left(\nabla F\left(\mathbf{r}_m\right)\right)^T \Delta\mathbf{r} + \frac{1}{2}\Delta\mathbf{r}^T B \Delta\mathbf{r} \tag{2.24}$$

where B is an approximation to the Hessian matrix H. The gradient of F with respect to the displacement $\Delta\mathbf{r}$ is

$$\nabla_{\Delta\mathbf{r}} F\left(\mathbf{r}_m + \Delta\mathbf{r}\right) \approx \nabla F\left(\mathbf{r}_m\right) + B\Delta\mathbf{r}. \tag{2.25}$$

Setting the gradient $\nabla_{\Delta\mathbf{r}} F = 0$, as it is the goal to minimise F with respect to a displacement $\Delta\mathbf{r}$, one gets

$$\Delta\mathbf{r} = -B^{-1} \nabla F\left(\mathbf{r}_m\right) \tag{2.26}$$

The $\Delta\mathbf{r}$ is used for a line search to arrive at a step size τ. The new position is then set to $\mathbf{r}_{m+1} = \mathbf{r}_m + \tau\Delta\mathbf{r}$.

In the BFGS algorithm the matrices B and $B^{-1} = D$ are updated by

$$B_{m+1} = B_m + \frac{\mathbf{y}_m\mathbf{y}_m^T}{\mathbf{y}_m^T\mathbf{s}_m} - \frac{B_m\mathbf{s}_m\mathbf{s}_m^T B_m}{\mathbf{s}_m^T B_m\mathbf{s}_m} \tag{2.27}$$

$$D_{m+1} = \left(I - \frac{\mathbf{s}_m\mathbf{y}_m^T}{\mathbf{y}_m^T\mathbf{s}_m}\right) D_m \left(I - \frac{\mathbf{y}_m\mathbf{s}_m^T}{\mathbf{y}_m^T\mathbf{s}_m}\right) + \frac{\mathbf{s}_m\mathbf{s}_m^T}{\mathbf{y}_m^T\mathbf{s}_m} \tag{2.28}$$

with $\mathbf{s}_m = \mathbf{r}_{m+1} - \mathbf{r}_m$ and $\mathbf{y}_m = \nabla F(\mathbf{r}_{m+1}) - \nabla F(\mathbf{r}_m)$.

The L-BFGS variant of the algorithm proposed by Bird et al.[18] is the default relaxation method in **exciting**[19] and most of the time results in fast improvements of the structure. It does however require a very accurate ground-state energy. If this method does not converge, the harmonic method is used.

2.3 Structure Optimisation

A structure optimisation for a tetragonal unit cell like rutile is done by changing either the volume of the unit cell or by changing the fraction c/a (COA). This is done by resizing the unit cell by a small parameter ε with the deformation matrices

$$M_{\text{Vol}} = \begin{pmatrix} 1+\varepsilon & 0 & 0 \\ 0 & 1+\varepsilon & 0 \\ 0 & 0 & 1+\varepsilon \end{pmatrix}$$

and

$$M_{\text{COA}} = \begin{pmatrix} \frac{1}{\sqrt{1+\varepsilon}} & 0 & 0 \\ 0 & \frac{1}{\sqrt{1+\varepsilon}} & 0 \\ 0 & 0 & 1+\varepsilon \end{pmatrix}.$$

By fitting the ground state energy depending on ϵ we obtain a unit cell with minimum energy. The fit functions are either a fourth-order polynomial for c/a-optimisation or the Birch-Murnaghan equation of state[20]

$$P(V) = \frac{3B_0}{2}\left[\left(\frac{V_0}{V}\right)^{\frac{7}{3}} - \left(\frac{V_0}{V}\right)^{\frac{5}{3}}\right]\left\{1 + \frac{3}{4}(B_0' - 4)\left[\left(\frac{V_0}{V}\right)^{\frac{2}{3}} - 1\right]\right\} \tag{2.29}$$

for the volume optimisation.

Because the optimum c/a value depends on the volume and vice versa, those optimisation have to be done alternately until a convergence is reached.

Example fits for a volume optimisation and c/a optimisation can be seen in Figure 2.1.

Figure 2.1: Fits for the structure optimisation

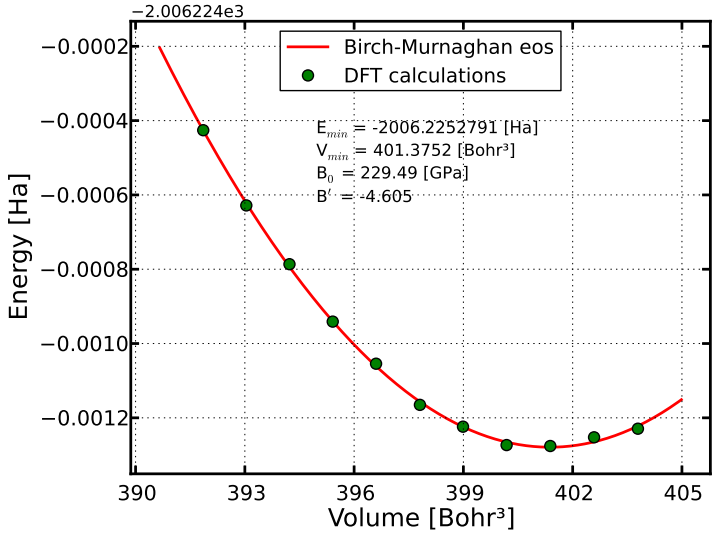

(a) Birch-Murnaghan equation of state fit for volume optimisation

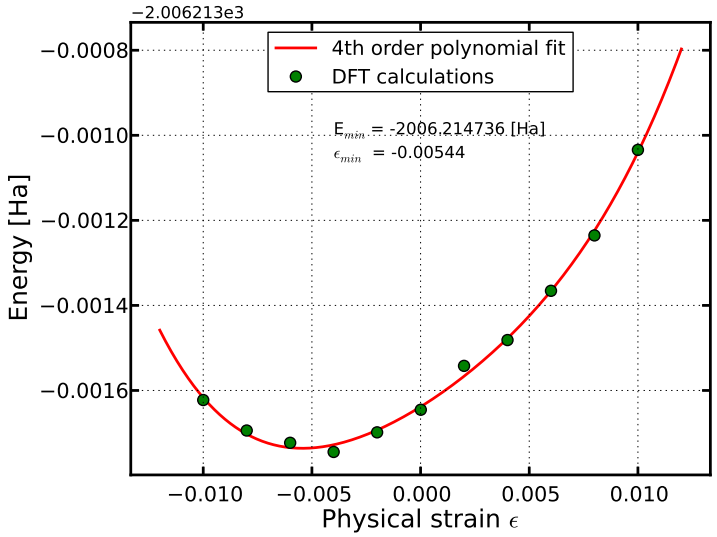

(b) Fourth-order polynomial fit for c/a optimisation

Chapter 3

Bulk Rutile

Rutile is the most common modification of TiO_2. The other rarer natural forms are anatase and brookite. Rutile is a tetragonal crystal with lattice parameters $a = b = 4.5936\,\text{Å}$ and $c/a = 0.64409$[21]. The inner parameter $u = 0.30479$[21] describes the distance of the oxygen atom to the neighbouring titanium atom in the unit cell. The unit cell is shown in Figure 3.1. The Ti ions are located at $(0, 0, 0)$ and $(1/2, 1/2, 1/2)$ and the O ions at $\pm(u, u, 0)$ and $\pm(u + 1/2, 1/2 - u, 1/2)$.

The experimental lattice values were the starting point for a structure optimisation using the version 'Beryllium' of the program **exciting**. The exchange-correlation potential used is GGA PBEsol by Perdew et al.[22].

3.1 Convergence Tests

For a meaningful structure optimisation, a set of converged parameters is a must. The two parameters for which convergence is especially important are `ngridk` and `rgkmax`.

`ngridk` determines the size of the k-point grid whereas `rgkmax` which stands for $R^{\text{MT}}_{\text{min}} |\mathbf{G} + \mathbf{k}|_{\text{max}}$ indirectly determines the maximum length of the $\mathbf{G}+\mathbf{k}$ vector. The maximum length of $\mathbf{G} + \mathbf{k}$ affects the size of the matrix Hamiltonian and therefore `rgkmax` determines the number of basis functions[19].

The muffin-tin radius `rmt` or R^{MT} defines the region around a nucleus where atomic-like wave functions are used. The smallest muffin-tin radius also determines the maximum length of the $\mathbf{G}+\mathbf{k}$ vector as described above. For oxygen the default

k-point grid	Number of irreducible k-points
1-1-2	2
2-2-3	6
2-2-4	9
3-3-5	9
3-3-6	12
4-4-6	24
4-4-7	24
5-5-7	24
5-5-8	30

Table 3.1: Number of irreducible k-points by k-point grid

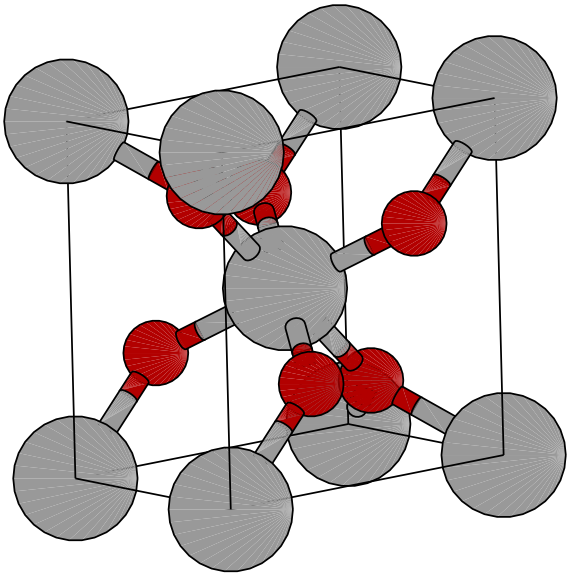

Figure 3.1: Unit cell of bulk rutile

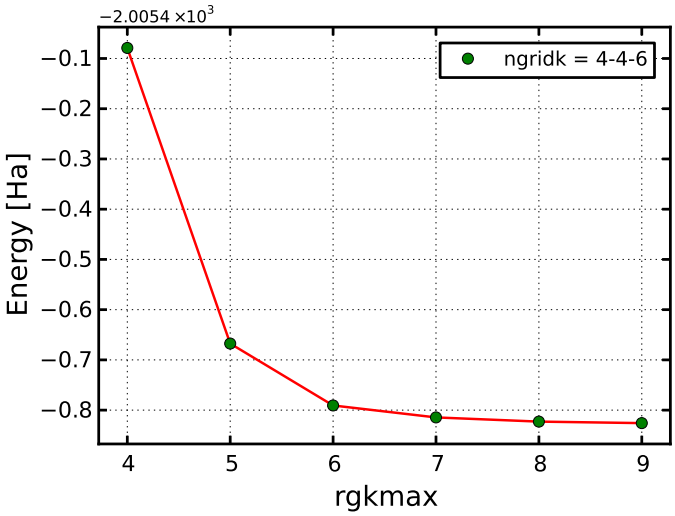

Figure 3.2: Convergence test in the parameter `rgkmax` for bulk rutile.

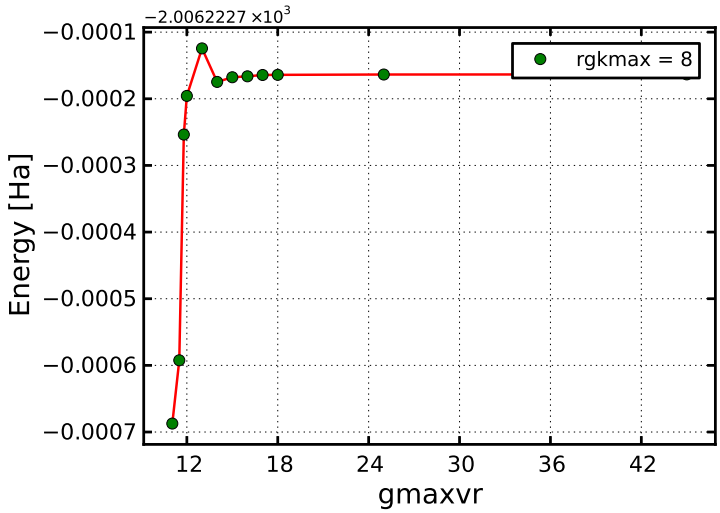

Figure 3.3: Convergence test in the parameter `gmaxvr` for bulk rutile.

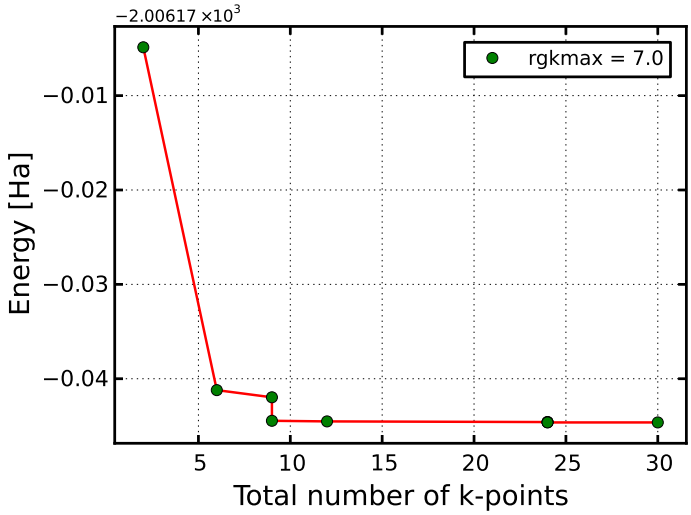

Figure 3.4: Convergence test in the number of k-points (reduced by crystal symmetries)

Property	experimental	calculated
a	4.5936 Å[21]	4.5349 Å
c	2.9587 Å[21]	2.8868 Å
u	0.30479[21]	0.3057
Band gap	~ 3 eV[25, 26]	3.6 eV (G_0W_0)

Table 3.2: Experimental and calculated properties of bulk rutile

muffin tin radius of $\texttt{rmt} = 1.45\, a_0$ has been used.

For the grid size **exciting** can also use another parameter `nktot`. It can be roughly set to a desired number of reducible k-points from which the program then determines a grid proportional to the inverse lattice vector length. For example $\texttt{nktot} = 100$ gives a 3-3-6 k-point grid. This number of reducible k-points is reduced by crystal symmetries. As can be seen in Table 3.1 the 3-3-6 k-point grid has 12 irreducible k-points.

As shown in Figures 3.2 and 3.4 a minimum $\texttt{rgkmax} = 6$ and a minimum of 12 k-points (that is a 3-3-6 k-point grid) are required for converged results.

The parameter `gmaxvr` has also been subject to convergence tests. Its value determines the length of $|\mathbf{G}|$. It has a lower bound of $\texttt{gmaxvr} > 2\texttt{gkmax} = 2\frac{\texttt{rgkmax}}{\texttt{rmt}_{\min}}$. In Figure 3.3 one can see that even the minimal value of $\texttt{gmaxvr} = 12$ has almost no effect on the energy.

Based on the results of the convergence tests, the calculations were performed with $\texttt{rgkmax} = 8$, $\texttt{gmaxvr} = 18$ and a 4-4-6 k-point grid.

3.2 Structure Optimisation

A structure optimisation as described in Section 2.3 was conducted. For every optimisation step a relaxation as described in Section 2.2.1 has been performed.

With this method a new optimised unit cell with parameters $a = 4.5349$ Å, $c = 2.8868$ Å and $u = 0.3057$ was found. The value of a and c is relatively small compared to the experimental value and calculations by Perron et al.[23] and Muscat et al.[24](both $a = 4.64$ Å, $c = 2.97$ Å). DFT calculations correspond to $T = 0$ K. However most experiments have been conducted at much higher temperatures. Therefore one would expect an expansion of the lattice constants in the experiment. The measurement by Abrahams et al.[21] was conducted at $T = 298$ K.

The calculated direct band gap at Γ is in agreement with the band gap of 3.46 eV calculated by Landmann et al.[27] also with PBE and G_0W_0 but using Vienna Ab-initio Simulation Package (VASP) instead of **exciting**. Calculations by Kang and Hybertsen[28] have also found a band gap close to the result in Table 3.2.

Chapter 4

(110) Surface of Rutile

It is known that rutile crystallises in such a way that 98 % of the crystal surface is composed of the (110), (101) and (100) planes. Of these the (110) plane makes up 60 % of the surfaces as measured by Jones et al.[29, 30]. It has the lowest density of dangling bonds[31, 32] making it the most stable surface.

4.1 Cutting the Surface

Using the program Atomistic Simulation Environment (ASE) the unit cell was cut at the (110) surface in 5 and 7 layers. An even number of layers was omitted because of its missing symmetry (Compare Figures 4.1 and 4.2).

The periodic boundary conditions **exciting** uses, make it necessary to add a vacuum large enough that two cells do not interact with one another. One problem arises when cutting the surface using ASE; one of the bridging oxygen atoms is placed on a wrong position so that one side of the slab has twice the amount of oxygen atoms than the other making the whole slab polar. This atom has to be manually placed on the other side of the surface (see Figure 4.2).

4.2 Version Change

Because of some convergence problems it was suggested to use the development version of **exciting** called 'Mortadella' which later became the version 'Boron'. This resulted in a speed up of the calculations as it takes less iterations to calculate the ground-state (GS) energy (see the comparison of different versions of **exciting** in Table 4.1). As we do not need the ground-state energy but only differences in energy, the change in versions should only have a negligible effect on the results.

Version	Number of iterations	Ground state energy [E_h]
'Lithium'	53	-10016.225
'Beryllium'	47	-10016.203
'Mortadella'	35	-10016.198
'Boron'	36	-10016.198

Table 4.1: Comparison of different versions of the program **exciting** with the default settings and `rgkmax` = 3, `ngridk` = $1 - 2 - 1$

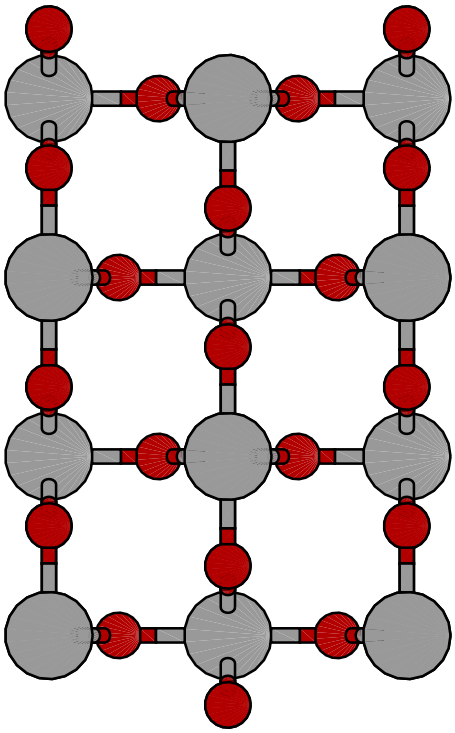

Figure 4.1: 4 layer rutile (110) slab

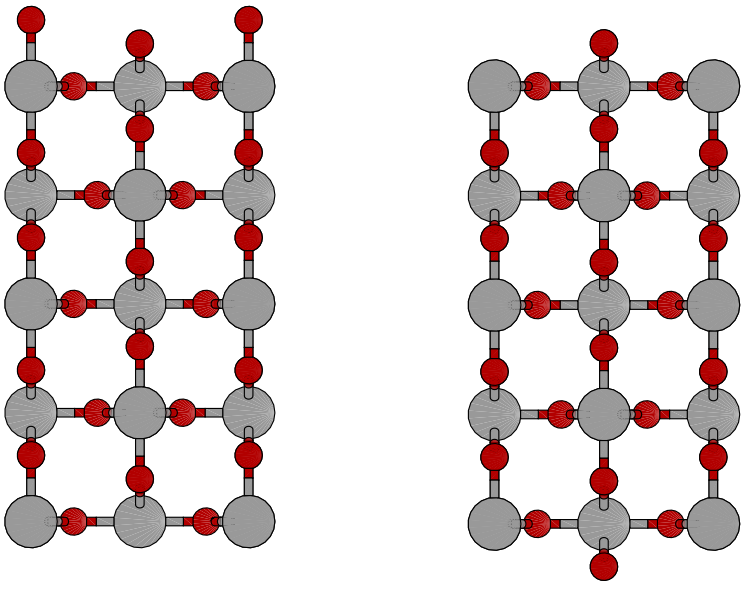

Figure 4.2: Wrongly cut surface (left) and manually corrected version (right)

k-point grid	Ground state energy [E_h]
2-4-1	-10030.676
2-4-2	-10030.677
2-4-3	-10030.677
2-4-4	-10030.677

Table 4.2: Ground-state energies of the slab for different numbers of k-points in the z-direction

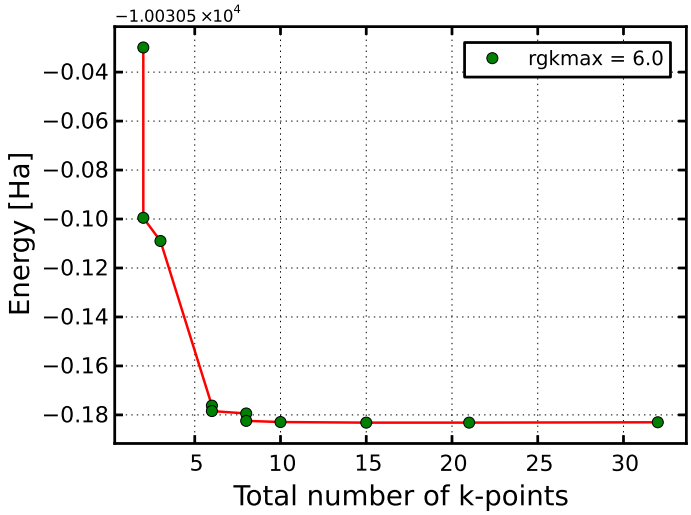

Figure 4.3: Ground-state energies of the slab for different numbers of irreducible k-points

4.3 Convergence Tests

As the surface unit cell differs from the bulk one it is unlikely that the same set of parameters yield converged results. Therefore a new series of convergence tests had to be made. As described in the previous Section 4.1 an additional convergence tests for the size of the vacuum had to be made.

Because of the large size of the unit cell containing 5 or 7 layers and vacuum, one k-point in the z-direction should suffice. This is confirmed by the results in Table 4.2.

The surface has fewer symmetries than the bulk therefore the number of k-points can not be reduced as much as before (See Table 4.3). As can be seen in Figure 4.3 the system yields already well converged results for a total number of 6 k-points, i.e. a 2-4-1 k-point grid. In Figure 4.4 one sees that `rgkmax` $= 8$ is converged well enough. Calculations with `rgkmax` > 8.35 did not finish because the ground-state energy calculation does not converge.

In Figure 4.5 one can see that as in the bulk material the value of `gmaxvr` has a negligible influence on the ground-state energy.

k-point grid	Number of irreducible k-points
1-2-1	2
1-3-1	2
1-4-1	3
2-4-1	6
2-5-1	6
2-6-1	8
3-7-1	8
3-8-1	10
4-9-1	15

Table 4.3: Number of irreducible k-points by k-point grid

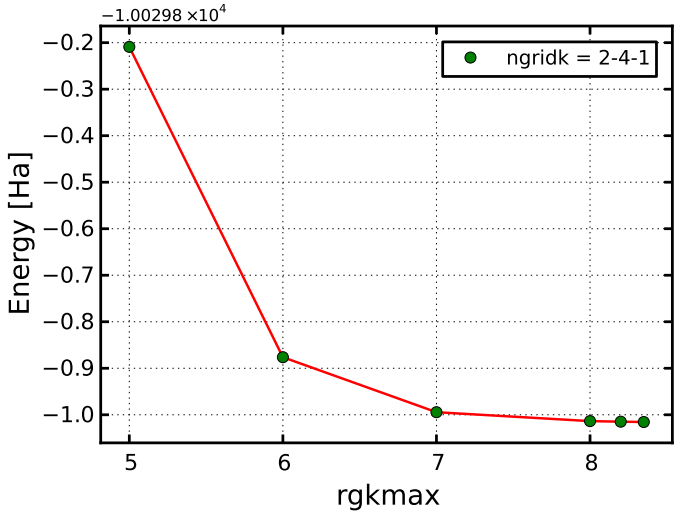

Figure 4.4: Ground-state energies of the slab for different values of `rgkmax`

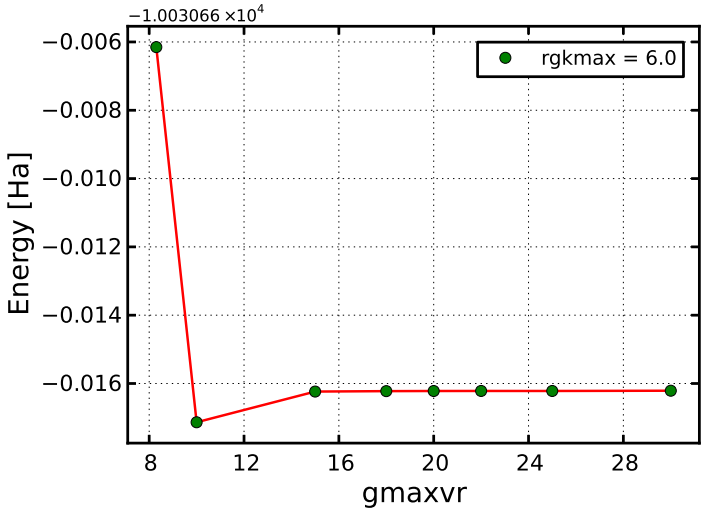

Figure 4.5: Ground-state energies of the slab for different values of `gmaxvr`

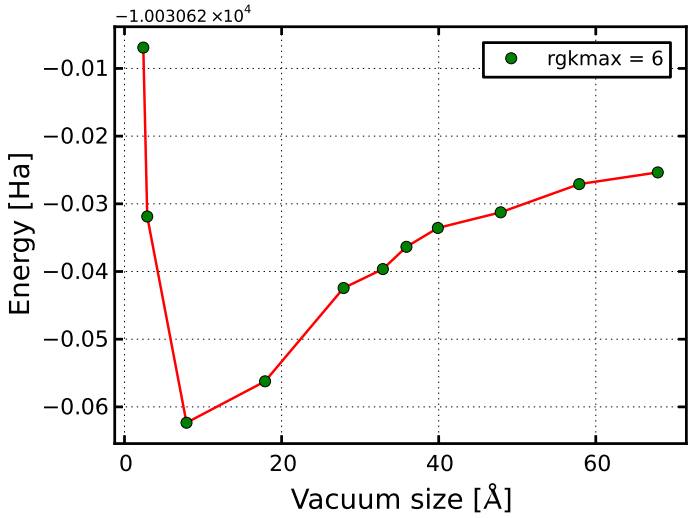

Figure 4.6: Ground-state energies of the slab for different vacuum sizes

4.3.1 Vacuum size

The convergence test in Figure 4.6 shows that the energy does not converge even for large vacuum sizes of more than 50 Å. However one can see that a vacuum size of about 8 Å between the two bridging oxygen atoms seems to be enough to have no repulsion because of the negative charge. In the calculations a vacuum size of 18 Å has been used.

4.4 Relaxing

It is unrealistic that the not optimised slab is anything like the real surface. The outer atoms relax to compensate the missing symmetry. Also surface reconstructions can happen which are not considered in this thesis.

Keeping a number of layers fixed is likely to speed up calculations as fewer atoms have to be considered. Fixated atoms also ensure some bulk-like character in the slab.

Two different approaches keep a number of layers fixed. The first is to relax only one side of the slab while keeping a few layers on the other side fixed. The other is to relax both sides and to fixate the inner layers.

Keeping one side fixed causes stresses on this side which increase the energy. This energy difference has to be considered when calculating the surface energy as has been done by Hameeuw et al.[33]. The break in symmetry also results in a polar slab.

The fixed inner layer (FIL) approach decreases the effective number of layers in the slab because half of the layers are symmetric to the other half and do not yield new information.

Even though this symmetry makes it necessary to use more layers for convergence, the FIL approach has been chosen because of its more physical nature and the easier to compute surface energies.

The symmetry of the cell should in theory speed up calculations but the relaxation code does not use them and actually breaks them by shifting the atomic

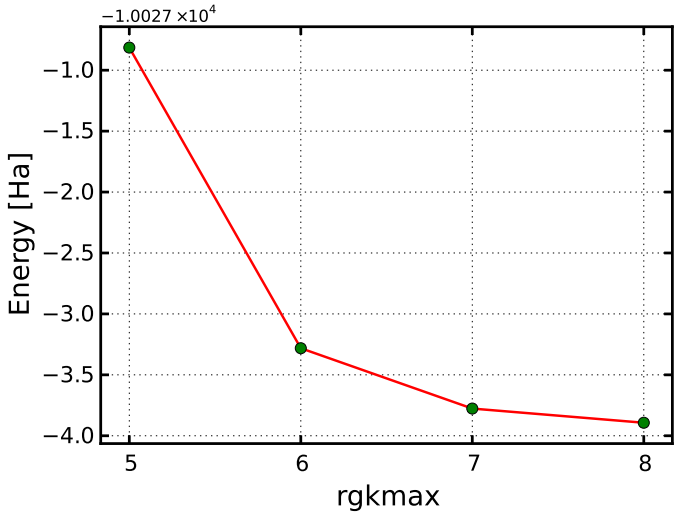

Figure 4.7: Ground-state energies after relaxation of a 5 layer (110) rutile slab with 3 layers fixated relaxed with different values of `rgkmax`

positions on both side of the slab by different values. Therefore the symmetry might only have some advantages in the first ground-state energy calculation and if manually restored for a later G_0W_0 calculation.

Because the bridging oxygen atom moves down to the slab but the underlying titanium atom up, the distance between those atoms gets smaller than the sum of both muffin-tin radii. Therefore the muffin-tin radius has to be decreased. This has been done with the titanium atom to keep the number of plane wave functions, which is indirectly determined by the smaller oxygen muffin-tin radius.

4.4.1 Relaxing the 5 Layer Rutile Slab

To relax the slab the inner layers were fixated and only the outer atoms were able to move. Starting with a high value for `rgkmax` would have resulted in very slow calculations. Therefore a lower value of `rgkmax` $= 5$ was chosen as a starting point. The configuration resulting from this calculation was then used as the starting point for a calculation with higher `rgkmax` and so forth. Even tough the value of `rgkmax` is not converged until the last iteration, the resulting configuration is closer to the equilibrium one than in the step before. For this reason the number of iterations necessary to relax the structure at high `rgkmax` becomes lower. A maximum force plot for `rgkmax` $= 5$ can be seen in Figure 4.8. In the beginning the BFGS method was used which yields very fast improvements. Because the method did not converge beginning with the sixth step the harmonic method was used.

The decrease in ground-state energy for each `rgkmax` step is shown in Figure 4.7 Based on the relaxed slab with 3 layers fixed, the same procedure was repeated for one and no layers fixed. The same approach has been used to relax a 7 layer slab. The ground-state energies for each step can be seen in Figure 4.9.

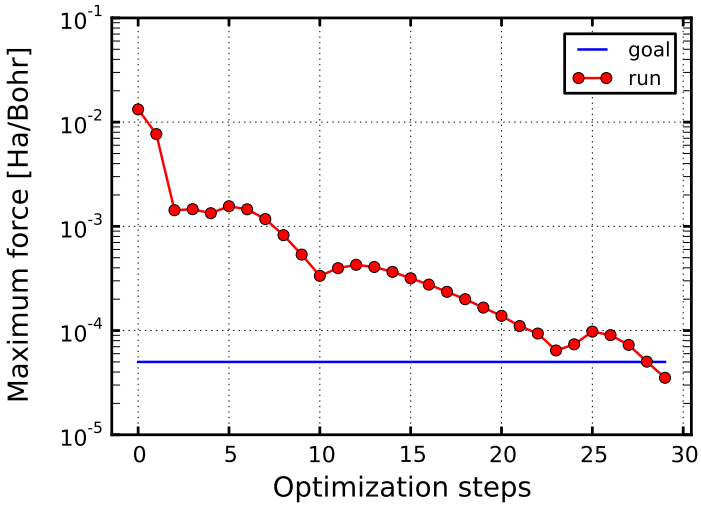

Figure 4.8: Maximum forces in the surface relaxation for each optimisation step of the 5 layer surface with 3 layers fixed and `rgkmax` = 5

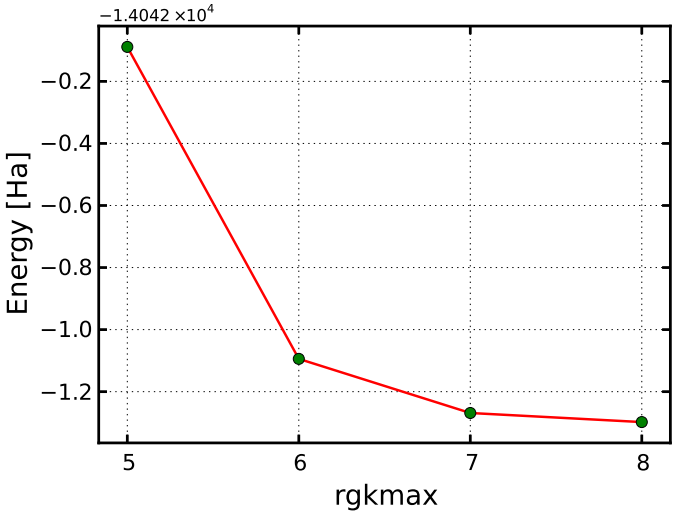

Figure 4.9: Ground-state energies after relaxation of a 7 layer (110) rutile slab with 3 layers fixated relaxed with different values of `rgkmax`

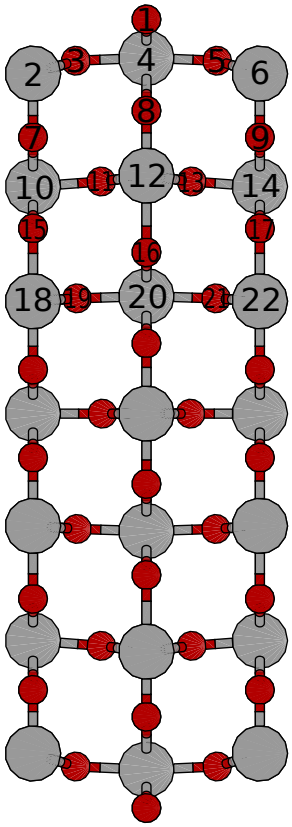

Figure 4.10: Position of atoms in the relaxed 7 layer rutile (110) slab

4.5 Displacement

Figure 4.10 shows the displacement of the atoms in a 7 layer slab. The numbers in Figure 4.10 correspond to the numbers in Table 4.5 and are the same for the 5 layer slab in Table 4.4.

Tables 4.4 and 4.5 show the bond lengths of the relaxed slabs. In the 5 layer slab one already gets well converged bond lengths if only one layer is fixed. However this is not true for the inner layers. Even in the 7 layer slab with only one fixed layer there is a change in bond length of about 1.5 % in the 18-23 bond and even about 3 % in the 20-24 bond. That means a higher number of layers in the slab might be needed for better results.

Results compiled by Thompson et al.[34] based on the experimental results of Charlton et al.[35] and Lindsay et al.[36] as well as calculated results by Bates et al.[37] are in very good agreement with the results for the 7 layer slab in Table 4.5. The differences in bond lengths between the fully relaxed 7 layer slab and the experimental values by Lindsay et al.[36] are about 0.05 Å.

4.6 Surface Energy Calculation

The surface energy is the energy difference between the surface and the bulk material with the same number of atoms. It can be obtained by

$$E_{\text{surf}} = \frac{E_{\text{slab}} - nE_{\text{bulk}}}{2A} \tag{4.1}$$

Bond	Bond length [Å]		
	5 layers, 3 fixed	5 layers, 1 fixed	5 layers, 0 fixed
1-4	1.8156	1.8082	1.8083
2-3	1.9036	1.9142	1.9145
3-4	2.0107	1.9996	2.0000
2-7	1.8433	1.8032	1.8039
4-8	2.0494	2.0754	2.0743
7-10	1.9068	1.9890	1.9886
8-12	1.9330	1.8620	1.8608
10-15	fixed	1.8753	1.8792
12-16	fixed	2.1283	2.1095
15-18	fixed	fixed	1.9859
16-20	fixed	fixed	1.9380

Table 4.4: Bond lengths of atoms in relaxed 5 layer slabs

Bond	Bond length [Å]		
	7 layers, 3 fixed	7 layers, 1 fixed	7 layers, 0 fixed
1-4	1.8072	1.8065	1.8063
2-3	1.9151	1.9188	1.9190
3-4	1.9987	1.9986	1.9982
2-7	1.8006	1.7967	1.7959
4-8	2.0768	2.0770	2.0782
7-10	1.9950	2.0062	2.0079
8-12	1.8553	1.8380	1.8369
10-15	1.8687	1.8670	1.8644
12-16	2.1588	2.1640	2.1794
15-18	fixed	2.0589	2.0645
16-20	fixed	1.9043	1.9014
18-23	fixed	1.9305	1.9150
20-24	fixed	1.9652	1.9748
23-26	fixed	fixed	1.9261
24-27	fixed	fixed	1.9811

Table 4.5: Bond lengths of atoms in relaxed 7 layer slabs

Layers	fixed	GS energy [E_h]	Energy per layer [E_h]	Surface energy [$\frac{\mathrm{J}}{\mathrm{m}^2}$]
5	5	-10030.84055	-2006.16811	1.397
	3	-10030.89936	-2006.17987	0.705
	1	-10030.91786	-2006.18357	0.487
	0	-10030.91974	-2006.18395	0.465
7	7	-14043,22467	-2006,17495	1.392
	3	-14043.30426	-2006.18632	0.455
	1	-14043.31283	-2006.18755	0.354
	0	-14043.31459	-2006.18780	0.334

Table 4.6: Ground-state and surface energies without and with relaxation of a different number of layers of (110) rutile slabs

Method	Layers	Surface energy $[\frac{\mathrm{J}}{\mathrm{m}^2}]$
GGA PW91[41]	9	0.58
GGA PW91[38]	11	0.58
GGA PBE[38]	11	0.49
GGA PBE[39, 40]	6	0.31
LDA[39]	6	0.84
LDA[31]	6	0.83
LDA[37]	7	0.73
LDA[42]	3	1.14
GGA PW[42]	3	0.82
GGA BP[42]	3	0.84
GGE PBEsol	7	0.33

Table 4.7: Comparison of the surface energy with other publications

with n being the number of layers and A the area of the surface. Because we have two surfaces on each side of the slab, the area is twice as large and therefore we have to use twice the area in the denominator. In the case of the (110) surface the area $A = \sqrt{2}ac$.

The change in **exciting** versions make it necessary to recalculate the ground-state energy of the bulk rutile. The slab ground-state energies were also recalculated using a finer 4-7-1 k-point grid. A new ground-state energy for the bulk material of $E_{\mathrm{bulk}} = 54.591\,\mathrm{keV}$ is obtained. With that and the unit cell parameters in Table 3.2 the surface energies have been calculated and are displayed in Table 4.6.

In Table 4.6 one can see that the surface energy is sensitive to lattice relaxation. This has also been shown by Kiejna et al.[38], Lazzeri et al.[39, 40]. The relaxed surface energies are in the same range as other GGA calculations[38–41] as can bee seen in Table 4.7.

Chapter 5

Discussion

Low-energy electron diffraction (LEED) images have shown that rutile (110) surfaces can be produced with almost no sign of surface reconstruction happening by annealing in ultra-high vacuum (UHV)[32]. This means that the major difference between bulk and surface of rutile is due to relaxation in the absence of defects.

In this thesis only an odd number of layers has been considered. Even though only 5 and 7 layer slabs were calculated, we see that the surface energy seems to decreases with the number of layers. This is in accordance with the findings of others[31, 37, 38] who observed the same behaviour for odd numbers of layers. They observed oscillations in surface energy between odd and even numbers of layers. For even numbers the surface energy increases. Odd and even layers converge to the same surface energy. Bates et al.[37] found that a number of at least 6 layers is needed to achieve convergence. This could not be verified because no 8 or 9 layer calculations have been done.

The choice to use GGA as exchange-correlation functional was based on the fact that PBEsol is designed to be especially accurate for bond lengths and lattice constants in transition metals like titanium[22]. For comparison the surface energies of the relaxed structure were calculated again with LDA as exchange correlation functional but keeping the surface structure the same as before (see Table 5.1). Comparing the results from LDA and GGA calculations, we see a difference in surface energies which is higher than the differences of Goniakowski et al.[42] who had calculated differences of about 30 %. Even though they found only small differences between LDA and GGA equilibrium surface positions, a relaxation of the investig-

Layers	fixed	Surface energy $[\frac{\mathrm{J}}{\mathrm{m}^2}]$
5	5	1.636
	3	0.994
	1	0.843
	0	0.834
7	7	1.627
	3	0.822
	1	0.777
	0	0.771

Table 5.1: Surface energies without and with relaxation of a different number of layers of (110) rutile slabs calculated with LDA

ated structure using LDA would likely produce lower values.

Bibliography

1. Phillips, L. G. & Barbano, D. M. The Influence of Fat Substitutes Based on Protein and Titanium Dioxide on the Sensory Properties of Lowfat Milks. *J. Dairy Sci.* **80,** 2726–2731. ISSN: 0022-0302 (Nov. 1, 1997).
2. Rutesh H. Dave. *Overview of pharmaceutical excipients used in tablets and capsules* Drug Topics. <`http://drugtopics.modernmedicine.com/drug-topics/news/modernmedicine/modern-medicine-news/overview-pharmaceutical-excipients-used-tablets`> (2008).
3. Fujishima, A. & Honda, K. Electrochemical Photolysis of Water at a Semiconductor Electrode. *Nature* **238,** 37–38 (July 7, 1972).
4. Sayama, K. & Arakawa, H. Effect of carbonate salt addition on the photocatalyticdecomposition of liquid water over Pt–TiO_2catalyst. *J. Chem. Soc., Faraday Trans.* **93,** 1647–1654. ISSN: 1364-5455 (Jan. 1, 1997).
5. Fox, M. A. & Dulay, M. T. Heterogeneous photocatalysis. *Chem. Rev.* **93,** 341–357. ISSN: 0009-2665 (Jan. 1, 1993).
6. Hoffmann, M. R., Martin, S. T., Choi, W. & Bahnemann, D. W. Environmental Applications of Semiconductor Photocatalysis. *Chem. Rev.* **95,** 69–96. ISSN: 0009-2665 (Jan. 1, 1995).
7. Mills, A., Davies, R. H. & Worsley, D. Water purification by semiconductor photocatalysis. *Chem. Soc. Rev.* **22,** 417–425. ISSN: 1460-4744 (Jan. 1, 1993).
8. Maness, P.-C. *et al.* Bactericidal Activity of Photocatalytic TiO_2 Reaction: toward an Understanding of Its Killing Mechanism. *Appl. Environ. Microbiol.* **65,** 4094–4098. ISSN: 0099-2240 (Sept. 1999).
9. Chang, C.-H. *et al.* Improved charge separation and transport efficiency in poly(3-hexylthiophene)–TiO_2nanorod bulk heterojunction solar cells. *J. Mater. Chem.* **18,** 2201–2207. ISSN: 1364-5501 (Apr. 30, 2008).
10. Bouclé, J. *et al.* Hybrid Solar Cells from a Blend of Poly(3-hexylthiophene) and Ligand-Capped TiO_2 Nanorods. *Adv. Funct. Mater.* **18,** 622–633. ISSN: 1616-3028 (Feb. 22, 2008).
11. Liao, W.-P., Hsu, S.-C., Lin, W.-H. & Wu, J.-J. Hierarchical TiO_2 Nanostructured Array/P3HT Hybrid Solar Cells with Interfacial Modification. *J. Phys. Chem. C* **116,** 15938–15945. ISSN: 1932-7447 (Aug. 2, 2012).
12. Hohenberg, P. & Kohn, W. Inhomogeneous Electron Gas. *Phys. Rev.* **136,** B864–B871 (Nov. 9, 1964).
13. Kohn, W. & Sham, L. J. Self-Consistent Equations Including Exchange and Correlation Effects. *Phys. Rev.* **140,** A1133–A1138 (Nov. 15, 1965).

14. Broyden, C. G. The Convergence of a Class of Double-rank Minimization Algorithms 1. General Considerations. *IMA J. Appl. Math.* **6,** 76–90. ISSN: 0272-4960, 1464-3634 (Mar. 1, 1970).

15. Fletcher, R. A new approach to variable metric algorithms. *Comput. J.* **13,** 317–322. ISSN: 0010-4620, 1460-2067 (Jan. 1, 1970).

16. Goldfarb, D. A family of variable-metric methods derived by variational means. *Math. Comp.* **24,** 23–26. ISSN: 0025-5718, 1088-6842 (1970).

17. Shanno, D. F. Conditioning of quasi-Newton methods for function minimization. *Math. Comp.* **24,** 647–656. ISSN: 0025-5718, 1088-6842 (1970).

18. Byrd, R., Lu, P., Nocedal, J. & Zhu, C. A Limited Memory Algorithm for Bound Constrained Optimization. *SIAM J. Sci. Comput.* **16,** 1190–1208. ISSN: 1064-8275 (Sept. 1, 1995).

19. *exciting input reference. exciting boron* Humboldt-Universität zu Berlin (July 2014). 108 pp. <`http://exciting-code.org/ref:input`>.

20. Birch, F. Finite Elastic Strain of Cubic Crystals. *Phys. Rev.* **71,** 809–824 (June 1, 1947).

21. Abrahams, S. C. & Bernstein, J. L. Rutile: Normal Probability Plot Analysis and Accurate Measurement of Crystal Structure. *J. Chem. Phys.* **55,** 3206–3211. ISSN: 0021-9606, 1089-7690 (Oct. 1, 1971).

22. Perdew, J. P. *et al.* Restoring the Density-Gradient Expansion for Exchange in Solids and Surfaces. *Phys. Rev. Lett.* **100,** 136406. ISSN: 0031-9007,1079-7114 (Apr. 4, 2008).

23. Perron, H. *et al.* Optimisation of accurate rutile TiO2 (110), (100), (101) and (001) surface models from periodic DFT calculations. *Theor. Chem. Acc.* **117,** 565–574. ISSN: 1432-881X, 1432-2234 (Apr. 1, 2007).

24. Muscat, J., Swamy, V. & Harrison, N. M. First-principles calculations of the phase stability of TiO_2. *Phys. Rev. B* **65,** 224112. ISSN: 1098-0121, 1550-235X (June 11, 2002).

25. Pascual, J., Camassel, J. & Mathieu, H. Fine structure in the intrinsic absorption edge of TiO_2. *Phys. Rev. B* **18,** 5606–5614. ISSN: 1098-0121, 1550-235X (Nov. 15, 1978).

26. Vos, K. & Krusemeyer, H. J. Low temperature electroreflectance of TiO_2. *Solid State Commun.* **15,** 949–952. ISSN: 0038-1098 (Sept. 1, 1974).

27. Landmann, M., Rauls, E. & Schmidt, W. G. The electronic structure and optical response of rutile, anatase and brookite TiO_2. *J. Phys.: Condens. Matter* **24,** 195503. ISSN: 0953-8984 (May 16, 2012).

28. Kang, W. & Hybertsen, M. S. Quasiparticle and optical properties of rutile and anatase TiO_2. *Phys. Rev. B* **82,** 085203. ISSN: 1098-0121, 1550-235X (Aug. 12, 2010).

29. Jones, P. & Hockey, J. A. Infra-red studies of rutile surfaces. Part 1. *Trans. Faraday Soc.* **67,** 2669–2678. ISSN: 0014-7672 (Jan. 1, 1971).

30. Jones, P. & Hockey, J. A. Infra-red studies of rutile surfaces. Part 2.—Hydroxylation, hydration and structure of rutile surfaces. *Trans. Faraday Soc.* **67,** 2679–2685. ISSN: 0014-7672 (Jan. 1, 1971).

31. Ramamoorthy, M., Vanderbilt, D. & King-Smith, R. D. First-principles calculations of the energetics of stoichiometric TiO_2 surfaces. *Phys. Rev. B* **49,** 16721–16727. ISSN: 1098-0121, 1550-235X (June 15, 1994).

32. Henrich, V. E. & Cox, P. A. *The Surface Science of Metal Oxides* 478 pp. ISBN: 9780521443890 (Cambridge University Press, Cambridge; New York, Mar. 3, 1996).

33. Hameeuw, K. J., Cantele, G., Ninno, D., Trani, F. & Iadonisi, G. The rutile TiO_2 (110) surface: Obtaining converged structural properties from first-principles calculations. *J. Chem. Phys.* **124,** 024708. ISSN: 0021-9606, 1089-7690 (Jan. 14, 2006).

34. Thompson, S. J. & Lewis, S. P. Revisiting the (110) surface structure of TiO_2: A theoretical analysis. *Phys. Rev. B* **73,** 073403. ISSN: 1098-0121, 1550-235X (Feb. 13, 2006).

35. Charlton, G. *et al.* Relaxation of TiO_2(110)-(1×1) Using Surface X-Ray Diffraction. *Phys. Rev. Lett.* **78,** 495–498. ISSN: 0031-9007, 1079-7114 (Jan. 20, 1997).

36. Lindsay, R. *et al.* Revisiting the Surface Structure of TiO_2(110): A Quantitative low-Energy Electron Diffraction Study. *Phys. Rev. Lett.* **94,** 246102. ISSN: 0031-9007,1079-7114 (June 22, 2005).

37. Bates, S. P., Kresse, G. & Gillan, M. J. A systematic study of the surface energetics and structure of TiO_2 (110) by first-principles calculations. *Surf. Sci.* **385,** 386–394. ISSN: 0039-6028 (Aug. 10, 1997).

38. Kiejna, A., Pabisiak, T. & Gao, S. W. The energetics and structure of rutile TiO_2(110). *J. Phys.: Condens. Matter* **18,** 4207. ISSN: 0953-8984 (May 3, 2006).

39. Lazzeri, M., Vittadini, A. & Selloni, A. Structure and energetics of stoichiometric TiO_2 anatase surfaces. *Phys. Rev. B* **63,** 155409. ISSN: 1098-0121, 1550-235X (Mar. 26, 2001).

40. Lazzeri, M., Vittadini, A. & Selloni, A. Erratum: Structure and energetics of stoichiometric TiO2 anatase surfaces [Phys. Rev. B 63, 155409 (2001)]. *Phys. Rev. B* **65,** 119901. ISSN: 1098-0121, 1550-235X (Feb. 15, 2002).

41. Harris, L. A. & Quong, A. A. Molecular Chemisorption as the Theoretically Preferred Pathway for Water Adsorption on Ideal Rutile TiO_2(110). *Phys. Rev. Lett.* **93,** 086105. ISSN: 0031-9007, 1079-7114 (Aug. 19, 2004).

42. Goniakowski, J., Holender, J. M., Kantorovich, L. N., Gillan, M. J. & White, J. A. Influence of gradient corrections on the bulk and surface properties of TiO_2 and SnO_2. *Phys. Rev. B* **53,** 957–960. ISSN: 1098-0121, 1550-235X (Jan. 15, 1996).

Acronyms

ASE Atomistic Simulation Environment

BFGS Broyden–Fletcher–Goldfarb–Shanno

DFT density functional theory

FIL fixed inner layer

GGA generalized gradient approximations

GS ground-state

LAPW linearized augmented planewave

LDA local density approximation

LEED low-energy electron diffraction

P3HT Poly(3-hexylthiophen-2,5-diyl)

TiO_2 titanium dioxide

UHV ultra-high vacuum

VASP Vienna Ab-initio Simulation Package

Selbständigkeitserklärung

Hiermit erkläre ich, dass ich die vorliegende Arbeit selbstständig und nur unter Zuhilfenahme der angegebenen Quellen und Hilfsmittel verfasst habe.